The EMBO Journal (2007) 26, 4391–4401 | © 2007 European Molecular Biology Organization | All Rights Reserved 0261-4189/07
www.embojournal.org

THE EMBO JOURNAL

Functional insights from structures of coactivator-associated arginine methyltransferase 1 domains

Nathalie Troffer-Charlier[1], Vincent Cura[1], Pierre Hassenboehler, Dino Moras and Jean Cavarelli*

Département de Biologie et Génomique Structurales, IGBMC (Institut de Génétique et de Biologie Moléculaire et Cellulaire) (UMR 7104 CNRS, U596 INSERM, ULP), Illkirch, France

Coactivator-associated arginine methyltransferase 1 (CARM1), a protein arginine methyltransferase recruited by several transcription factors, methylates a large variety of proteins and plays a critical role in gene expression. We report, in this paper, four crystal structures of isolated modules of CARM1. The 1.7 Å crystal structure of the N-terminal domain of CARM1 reveals an unexpected PH domain, a scaffold frequently found to regulate protein–protein interactions in a large variety of biological processes. Three crystal structures of the CARM1 catalytic module, two free and one cofactor-bound forms (refined at 2.55 Å, 2.4 Å and 2.2 Å, respectively) reveal large structural modifications including disorder to order transition, helix to strand transition and active site modifications. The N-terminal and the C-terminal end of CARM1 catalytic module contain molecular switches that may inspire how CARM1 regulates its biological activities by protein–protein interactions.

The EMBO Journal (2007) **26,** 4391–4401. doi:10.1038/sj.emboj.7601855; Published online 20 September 2007
Subject Categories: chromatin & transcription; structural biology
Keywords: CARM1; coactivator-associated arginine methyltransferase 1; nuclear receptor coactivator; PRMT; protein ariginine methylation

Introduction

Post-translational methylation of arginine is a widespread epigenetic modification found in eukaryotes that is catalyzed by the protein arginine methyltransferases (PRMTs). PRMTs have been implicated in a variety of biological processes, such as regulation of transcription, translation and DNA repair (Bedford and Richard, 2005; Pahlich *et al*, 2006; Krause *et al*, 2007). PRMTs transfer the methyl group from *S*-adenosyl-L-methionine (SAM, also known as AdoMet) to the side chain nitrogens of arginine residues to form methylated arginine derivatives and *S*-adenosyl-L-homocysteine (SAH, also known as AdoHcy). At least nine members of PRMTs (PRMT1 to PRMT9) have been identified and classified into two main classes (type I and II PRMTs). Both classes catalyze the formation of monomethylarginine as intermediate. In a second step, type I PRMTs (PRMT1, PRMT3, PRMT4 and PRMT6) form asymmetric dimethylarginine, whereas type II form symmetric dimethylarginine. Coactivator-associated arginine methyltransferase 1 (CARM1, also known as PRMT4) was identified as an enhancer of the transcriptional activation by several nuclear hormone receptors (NRs) (Chen *et al*, 1999). CARM1 transcriptional regulation is done by methylation of histone H3 (on Arg2, Arg17 and Arg26) and by protein–protein interactions with the p160 family of coactivators. As a transcriptional coactivator, CARM1 is a key player in the formation of large complexes on gene promoters leading to chromatin remodelling and gene activation (Lee *et al*, 2002; Xu *et al*, 2004; Feng *et al*, 2006; Naeem *et al*, 2007). It has been proposed that CARM1 may play a dual function first by activating transcription by modifying core histone tails and then by facilitating disassembly of the coactivator complex (Feng *et al*, 2006).

CARM1 has now been shown to methylate a large variety of proteins which are all vital to gene expression (for a recent review, see Wysocka *et al*, 2006). Those CARM1 substrates can be broadly divided into two classes: (i) proteins that are involved in chromatin remodelling (such as histone H3 and the 300 kDa cAMP response element-binding protein (CREB)-binding protein (CBP)) and (ii) proteins that possess RNA-binding properties (such as PABP1, TARPP, HuR and HuD) and splicing factors (such as CA510, SAP49, SmB and U1C) (Cheng *et al*, 2007). CARM1 has been shown to be recruited by several transcription factors and therefore plays a critical role in gene expression as a positive regulator.

CARM1 contains 608 amino acids in mouse (and human) and its architecture has been schematically divided into three domains. CARM1 is built around a catalytic core domain (residues 150–470 in mouse CARM1 (mCARM1)) that is well conserved in sequence (and therefore in structure) among all PRMTs members (for recent reviews, see Cheng *et al*, 2005; Krause *et al*, 2007). CARM1 possesses two unique additional domains attached, respectively, at the N-terminal and at the C-terminal end of the PRMT active site (Figure 1). Both N-terminal domain (residues 1–130 in mCARM1) and C-terminal domain (residues 480–608 in mCARM1) have been shown to be required for the coactivator function of human CARM1 (Teyssier *et al*, 2002).

We report in this study the structure determination and the structural analysis of four crystal structures corresponding to three isolated modules of mouse CARM1: $CARM1_{28–140}$, $CARM1_{140–480}$ and $CARM1_{28–507}$. $CARM1_{28–140}$ (residues 28–140 of mCARM1) has been solved and refined at a resolution of 1.7 Å, while the structure of $CARM1_{28–507}$ (residues 28–507

*Corresponding author. Laboratoire de Biologie et Génomique Structurales, IGBMC (CNRS/INSERM/ULP), 1 rue Laurent Fries, BP 10142, Ilkirch 67404, France. Tel.: +33 388 65 5793; Fax: +33 388 65 3276; E-mail: cava@igbmc.u-strasbg.fr
[1]These authors contributed equally to this work

Received: 11 June 2007; accepted: 21 August 2007; published online: 20 September 2007

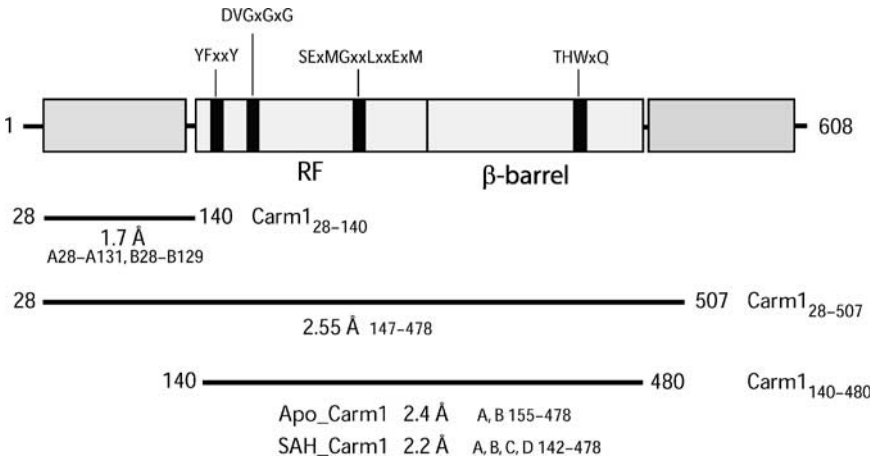

Figure 1 Schematic diagram illustrating the modular organization of full-length CARM1. Three structural domains are highlighted: the catalytic core module, composed of two parts (a Rossmann fold topology (RF) and a β-barrel), is very well conserved among PRMTs members; additional domains attached respectively at the N-terminal and at the C-terminal side of the PRMT active site. The borders of each domain are indicated for mouse CARM1. The location of the four PRMT conserved motifs is also indicated. The isolated domains of CARM1 whose structure has been solved and refined in this work are shown: resolution of the X-ray data and ordered residues in each domain are indicated.

Table I Crystallographic data and refinement statistics

	$CARM1_{28-140}$	$CARM1_{28-507}$	$CARM1_{140-480}$	$SAH–CARM1_{140-480}$
Space group	$P4_12_1$ 2	$P6_22$ 2	I222	$P2_12_12$
Unit cell parameters				
a, *b*, *c* (Å)	46.1, 46.1, 201.3	136.0, 136.0, 125.3	73.8, 98.1, 207.1	74.5, 98.2, 206.05
Resolution (Å)	42.0–1.69 (1.74–1.69)	50–2.55 (2.63–2.55)	30.0–2.4 (2.46–2.4)	30.0–2.2 (2.25–2.20)
Unique reflections	25 232	21 499	28 039	74 162
Completeness (%)	99.4 (99.9)	99.1 (99.4)	99.0 (95.0)	99.5 (96.4)
Number of atoms	1870	2785	5233	11 400
Rcryst, Rfree (%)[a]	20.5 (25.5)	23.0 (26.9)	20.5 (26.5)	18.6 (23.9)
Bonds (Å)/angles (deg)[b]	0.011/1.2	0.015/1.6	0.012/1.4	0.015/1.5
Average B factor	18.6	46.8	45.0	32.1

Numbers in parentheses indicate statistics for the high-resolution data bin.
[a]$R = \Sigma_{hkl}|Fobs - Fcalc|/\Sigma_{hkl}$ Fobs where Fobs and Fcalc are the observed and calculated structure factor amplitudes for reflection hkl, applied to the work (Rfactor) and test (Rfree) sets, respectively. For each data set, the test set contains 5% of the data set.
[b]R.m.s. deviations were calculated using Engh and Huber parameters (Engh and Huber, 1991).

of mCARM1) has been solved and refined at 2.55 Å resolution. The structure of $CARM1_{140-480}$ (residues 140–480 of mCARM1) has been determined in two different biological states: an apo form (at 2.4 Å resolution) and an SAH-$CARM1_{140-480}$ form (at 2.2 Å resolution) with the SAH molecule bound in the catalytic active site.

Results and discussion

$CARM1_{28-140}$ reveals an unexpected PH domain-like fold and behaves as a dimer

$CARM1_{28-140}$ was expressed in *Escherichia coli*, purified and crystallized. The structure has been solved and refined at 1.7 Å (see Supplementary data for structure determination details and Table I for crystallographic statistics). $CARM1_{28-140}$ adopts a β-sandwich fold (Figure 2A) that contains two nearly orthogonal β-sheets made up of seven antiparallel β-strands and is capped by a C-terminal amphipatic α-helix (residues 115–128). Strands β_1 to β_4 (residues 31–42, 49–63, 67–73 and 79–86) form a β-sheet (β_{1-4}) that is almost orthogonal to a second β-sheet (β_{5-7}) containing strands β_5 to β_7 (residues 90–94, 98–103 and 106–111). As strands β_1 and β_2 contribute to both sheets, the overall structure has an opened-barrel appearance. Two monomers of $CARM1_{28-140}$ are present in the crystallographic asymmetric unit and the dimer interface is made up by β-sheet β_{5-7} of each monomer (Figure 2B). The dimer interface corresponds to a buried surface area of 1002 $Å^2$ (using a sphere radius of 1.4 Å), which represents approximatively 15% of the total accessible surface area of an isolated monomer. It is noteworthy that during the purification and characterization process $CARM1_{28-140}$ always behaves as a dimeric entity as shown by native gel electrophoresis, mass spectrometry under non-denaturing conditions, analytical ultracentrifugation (see Supplementary data). Nevertheless, the biological relevance of $CARM1_{28-140}$ dimer requires further investigations.

A search of the Protein Data Bank using the Dali server (Holm and Sander, 1995) at EBI revealed that $CARM1_{28-140}$ is highly similar to a family of *Drosophila*-enabled/vasodilator-stimulated phosphoprotein homology 1 (EVH1) domains, which includes protein Mena (PDB entry 1EVH; Z-score 12.6), Ran-binding protein (RanBP, PDB entry 1RRP; Z-score 10.6) and Dcp1p, a decapping protein involved in mRNA degradation (PDB entry 1q67; Z-score 10.2). EVH1 domains belong to the superfamily of 'pleckstrin homology domain' (PH) fold that is built up by two perpendicular antiparallel β-sheets followed by a C-terminal amphipatic helix. The loops connecting the β-strands differ greatly in

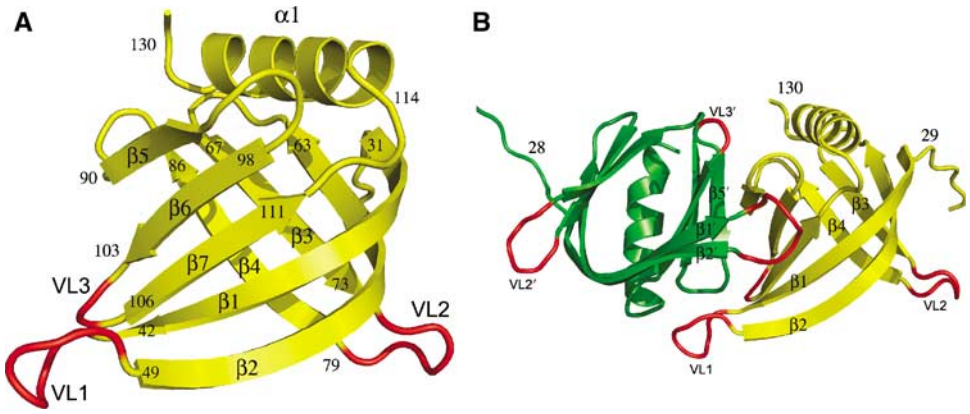

Figure 2 Structure of $CARM1_{28–140}$. (**A**) Overview of one monomer illustrating the PH domain fold. Strands β1 through β7 and the C-terminal helix α1 are labelled. The loops between β1 and β2 (VL1), between β3 and β4 (VL2), between β6 and β7 (VL3), which are variable in size and conformation in known PH domains, are also indicated. (**B**) Overview of the noncrystallographic dimer. The interface is made up by β-sheet $\beta_{5–7}$ of each monomer. This dimer interface observed in $CARM1_{28–140}$ usually builds up the ligand-binding site of other PH domains.

length in all known structures. EVH1 domains comprise an important family of protein interaction domains which have been shown to be located exclusively at the N-terminal end of larger modular proteins and specifically bind to target proline-rich sequences with low affinity and high specificity (Ball *et al*, 2002, 2005). The few highly conserved surface-exposed aromatic side chains that are characteristic of EVH1 domains are not present in CARM1. Moreover, the surface buried at the interface of the $CARM1_{28–140}$ dimer hides the ligand-binding site found in all PH domains (Figure 2B).

To date, PH domain-like fold contains nine families in SCOP (Murzin *et al*, 1995) and includes proteins involved in a variety of biological processes such as signal transduction, cytoskeletal organization, nuclear transport and DNA repair (Blomberg *et al*, 1999; Ball *et al*, 2002; Lemmon *et al*, 2002; Gervais *et al*, 2004; She *et al*, 2004; Lemmon, 2007). This superfamily contains proteins that share a highly similar fold in spite of insignificant sequence similarity. The PH domain constitutes one of the most common tools used by nature to build larger proteins and to regulate protein–protein associations. This scaffold has been shown to provide low affinity and high specificity in multiprotein complexes involved in biological events that require association and dissociation of proteins in response to external stimuli. CARM1 has been shown to interact with a large repertoire of proteins and to be involved in many multiprotein complexes that all impact gene expression. Therefore, it may not be so surprising to discover such a precious structural tool in this versatile protein. As presented below, $CARM1_{28–140}$ does not interact with the catalytic domain. To the best of our knowledge, local interactions involving the N-terminal domain and a protein partner have not yet been identified. Therefore, if $CARM1_{28–140}$ dimer is not biologically relevant, the ligand recognized by CARM1 PH domain will differ from those already known and remains to be discovered.

CARM1 PRMT catalytic module

SAH-$CARM1_{140–480}$ (residues 140–480 of mCARM1 in complex with SAH) will be used as reference for the further analysis and discussion of the catalytic domain of mCARM1. The core catalytic domain of CARM1 (residues 150–470) is very well conserved in sequence among all PRMTs (for recent reviews, see Cheng *et al*, 2005; Krause *et al*, 2007) and was therefore expected to be similar in structure with the already known structures of rat PRMT1 (PDB entries 1OR8, 1ORI and 1ORH) (Zhang and Cheng, 2003), rat PRMT3 (PDB entry 1F3L) (Zhang *et al*, 2000) and yeast RMT1/Hmt1(Weiss *et al*, 2000; Figure 3). The catalytic module of CARM1 is indeed folded into two domains connected by a conserved *cis*-proline residue (Pro288) and divided into four parts (Figure 4). The first domain at the N-terminal end contains a typical Rossmann Fold (yellow, residues 166–287) and two terminal helices (pink, named as αX (residues 144–154) and αY (residues 157–164) following the convention used for rat PRMT3 catalytic core (Zhang *et al*, 2000)). The second domain is a β-barrel (green, residues 290–299 and residues 378–478) to which an arm containing a four-helix segment (blue, residues 300–338) is added. This arm has been shown to be involved in the dimerization of PRMTs. The Rossmann fold domain that harbors the AdoMet consensus fold conserved in AdoMet-dependent methyltransferases (Martin and McMillan, 2002) contains four helices (named A, B, D, Z and Z′) and 5 strands (named β1 to β5). Two of the four PRMTs signature sequences referred in this paper as motif I ($Y_{150}F_{151}xxY_{154}$, numbered as in mCARM1) and motif II ($D_{191}V_{192}G_{193}xG_{195}xG_{197}$) belong to the first domain. In $CARM1_{140–480}$, the β-barrel contains 11 strands (named β6 to β16) and 6 helices (E, F, G′, G, H and I). This domain harbors the two other signature sequences referred in this paper as motif III ($S_{257}E_{258}xM_{260}G_{261}xxL_{264}xxE_{267}xM_{269}$, also known as double E-loop) and motif IV ($T_{414}H_{415}W_{416}xQ_{418}$).

$CARM1_{140–480}$ differs from the already known PRMT catalytic domain structures by three unique features located respectively at (i) the N-terminal end, (ii) the C-terminal end and (iii) in the dimerization arm of the protein. Except that, the core catalytic domain of CARM1 is indeed very similar in structure with the already known PRMT catalytic domain structures. Superimposing SAH-$CARM1_{140–480}$ on the three other PRMT structures gives r.m.s. deviation in the range of 1.4–1.6 Å between corresponding 296 Cα atoms. As discussed below, residues 141–170 of CARM1 are the site of structural changes, including order-to-disorder transition and secondary structure conformational changes. Strand β16 of CARM1 (residues 472–478) has not been observed in other known PRMTs structures, as the C-terminal end of

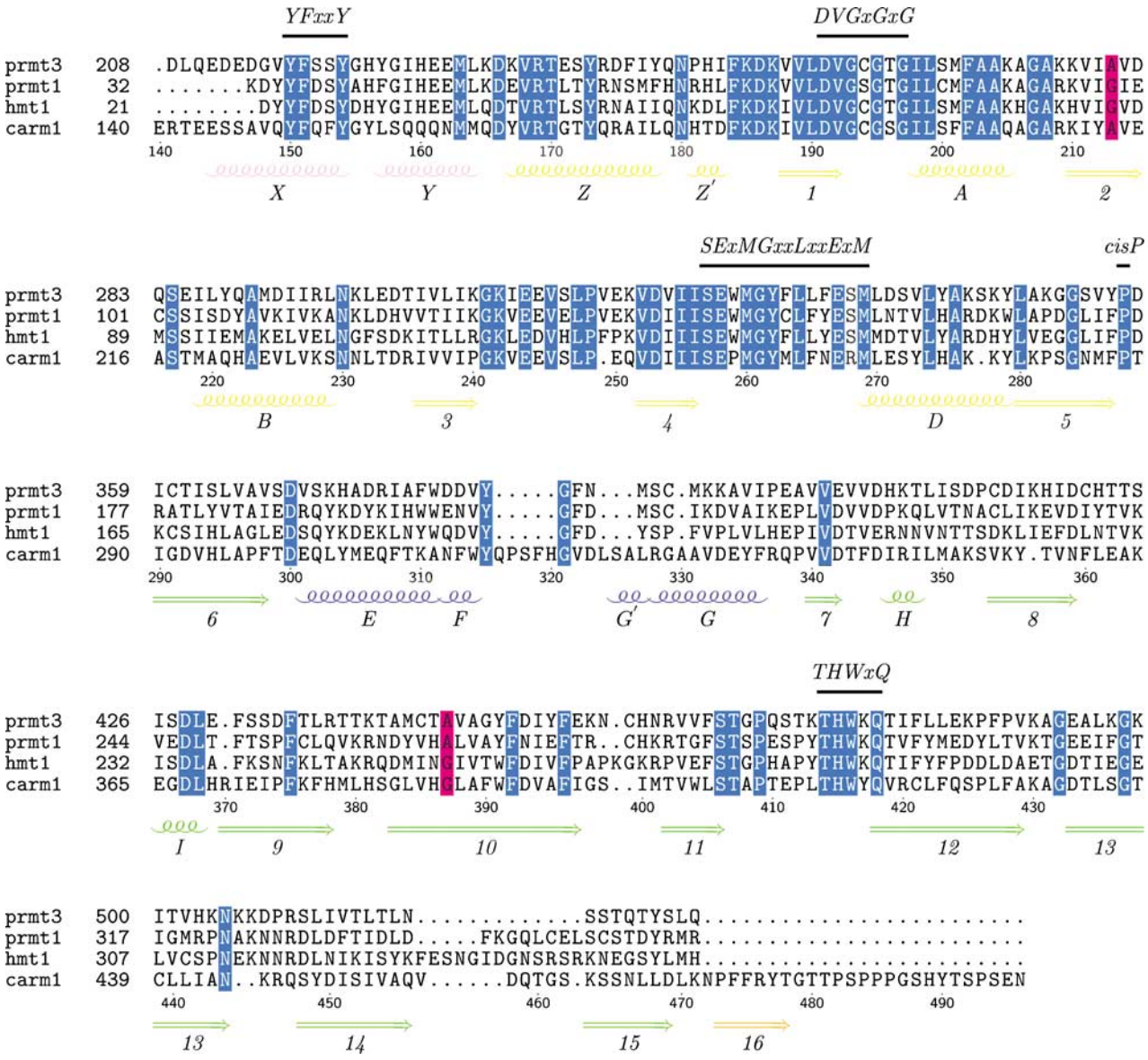

Figure 3 Structure-based sequence alignment for rat PRMT1, rat PRMT3, yeast RMT1/Hmt1 and mCARM1. The secondary structure is displayed for mCARM1; the color coding is described in the text. The mCARM1 residue numbering is shown below the sequences. The four motifs characteristic of the PRMT domain are shown. Amino acids highlighted are either invariant (blue) or similar (violet) as defined by the following grouping: F, Y and W; I, L, M and V; R and K; D and E; G and A; S, T, N and Q. Helices and strands are labelled as described in the text. This figure was produced with the program TeXshade (Beitz, 2000).

other known PRMTs (Arg353 of PRMT1, Gln528 of PRMT3 and His348 of RMT1/Hmt1) corresponds to residue Lys471 of CARM1. Strand β16 belongs to the β-sheet formed by strands β7-β12-β11-β10-β6-β8. The active site entrance is therefore delineated on one side by helices αX and αY, on the top by helix αZ and by the loop of motif IV, and on the other side by strand β16. Finally, in contrast to PRMT1 and PRMT3, the dimerization arm of $CARM1_{140–480}$ contains an insertion peptide of 10 residues that modifies the relative orientation of the two monomers in the dimer. This arm contains two α-helices (named E and G) and two short 3_{10}-helices (named F and G′).

S-adenosyl-L-homocysteine-binding site

The structure of SAH-$CARM1_{140–480}$ refined at 2.2 Å resolution confirms and extends what was already known from PRMT1 and PRMT3 structures. The SAH molecule is buried in a deep pocket located between the carboxyl end of the parallel β strands 1, 2 and 4 and the N-terminal helices (αX, αY and αZ) (Figure 5A and B). The cofactor is surrounded by all four PRMTs signature sequences and the interactions have been generally classified according to the three moieties of SAH. For the methionine moiety, Arg169 (of helix αZ) interacts with the carboxylate atoms and with Glu258 of motif II, while the amino group interacts on one side with the oxygen atom of Gly193 and on the other side with Asp191 of strands β1 via a water molecule, both residues belonging to motif I. For the ribose moiety, both hydroxyls are mainly recognized by Glu215 at the end of strand β2. For the adenine ring moiety, nitrogens N6, N1 and N7 interact, respectively, with Glu244 (loop after strand β3) and Ser272 (helix αD), the main-chain nitrogen atom of Val243, and with a water

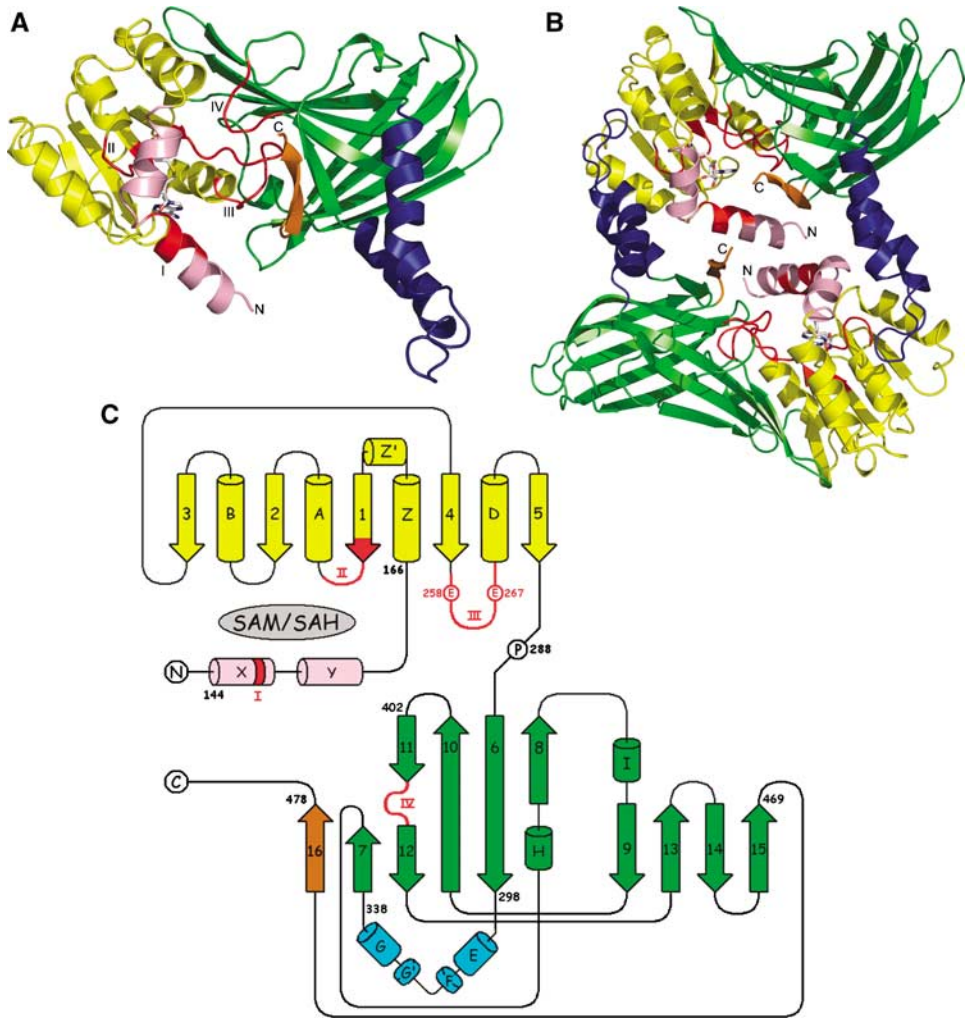

Figure 4 The structure of SAH-CARM1$_{140–480}$. (**A**) Overview of one monomer. The SAH/SAM-binding domain is shown in yellow, the N-terminal helices αX and αY in pink, the β-barrel in green, the dimerization arm in blue, the last C-terminal strand in orange. The bound SAH molecule is shown in a stick model and the four motifs characteristic of PRMT domain (I, II, III and IV) are highlighted in red. (**B**) Ribbon representations of SAH-CARM1$_{140–480}$ dimer formed by interactions between the dimerization arm of monomer 1 with the outer surface of the Rossmann fold moiety of monomer 2. (**C**) Topology diagram of the secondary structure elements. The color code defined in (A) is also used here.

molecule. This water molecule also interacts with Ser272 mentioned above. The binding site of the arginine substrate, observed in PRMT1 structure, is occupied by ordered water molecules.

The co-factor molecule is firmly locked and buried by three of the four aromatic rings of motif I. Tyr154 of motif I interacts with Glu267, a conserved residue that has been shown to be crucial for the protein methyltransferase activity (Lee *et al*, 2002). Therefore, as discussed below, structural changes of the N-terminal helices (αX, αY and αZ) are required during the catalytic pathway. The Tyr154–Glu267 interaction, involving two invariant residues in the PRMTs sequences, may therefore be one of the clues that control the catalytic reaction.

Order-to-disorder transition upon SAH binding on CARM1$_{140–480}$

In the absence of cofactor, the structure of CARM1$_{140–480}$ (apo-CARM1$_{140–480}$) reveals that residues 144–154 which will build up the N-terminal helix αX of SAH-CARM1$_{140–480}$ are not seen in the electron density map of apo-CARM1$_{140–480}$ and are therefore probably disordered (Figure 5C). The other noticeable structural change concerns the conformations of two residues of motif II (Gly195 and Ser196) and of the loop between helix F and G′ of the dimerization arm. Interestingly, there are no conformation changes of the backbone of the loops of motifs III and IV upon SAH binding. Moreover, in apo and holo CARM1$_{140–480}$, the conformation of the loops of motifs III and IV are very similar compared to SAH-PRMT1 (PDB entries 1OR8, 1ORI and 1ORH) (Zhang and Cheng, 2003), rat SAH-PRMT3 (PDB entry 1F3L) (Zhang *et al*, 2000) and yeast apo RMT1/Hmt1(Weiss *et al*, 2000). The conserved backbone conformations seem therefore to be a prerequisite for catalytic activity. The only difference in the backbone conformation of motif III concerns the residue corresponding to Arg268 in CARM1 that is located between the conserved Glu267 and Met269. Two conformations are observed in all known crystal structures; a 'down' conformation as observed in CARM1 (Arg268) and PRMT3 (Ser336) and an 'up' conformation as observed in PRMT1 (Ser 154) and RMT1/Hmt1

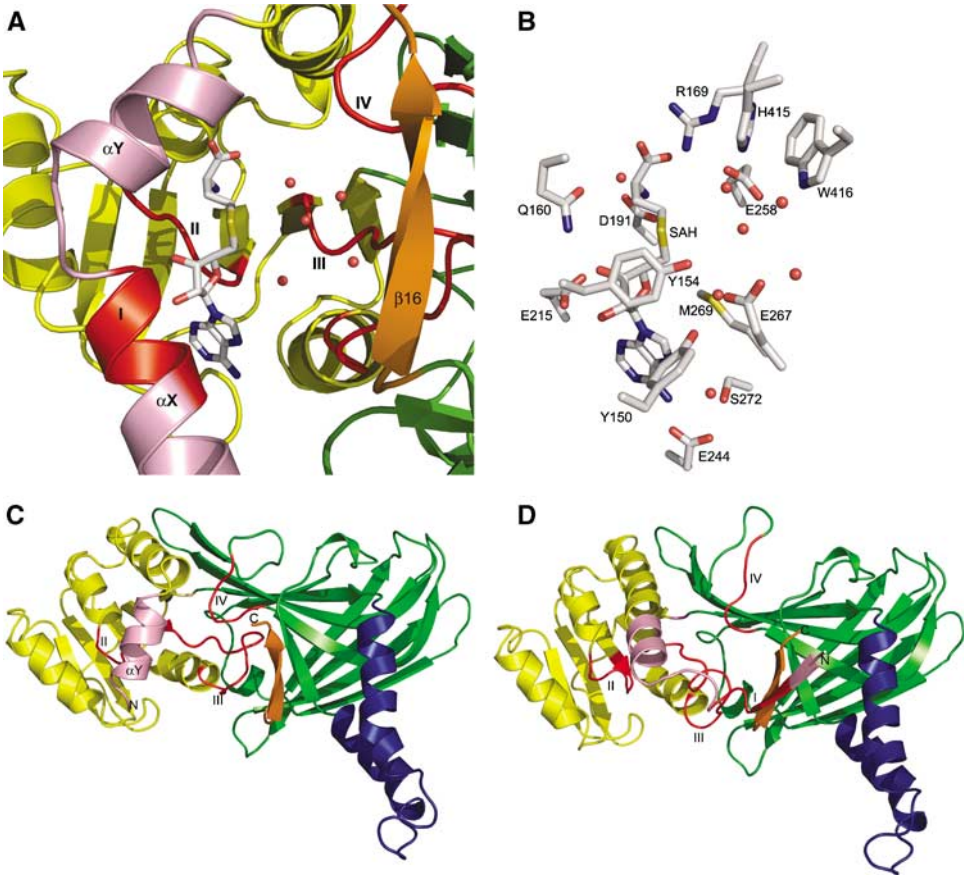

Figure 5 PMRT catalytic site of CARM1. (**A**) Overview of the SAH-binding site. Backbone conformations of the loops of motifs I to IV are highlighted in red. The ordered water molecules which occupy the binding site of the arginine substrate are shown as red spheres. (**B**) SAH recognition: interactions between some active-site residues and SAH. SAH molecule and some key interacting side chains are shown as stick representations. (**C**) apo-CARM1$_{140–480}$: residues 144–154 of helix αX of SAH-CARM1$_{140–480}$ are disordered. (**D**) CARM1$_{28–507}$. Part of helix αX has been changed in a strand β0 and the kink between helices αY and αZ has disappeared, helices αY and αZ have been merged together. Strand β0 forms a two-stranded antiparallel β-sheet with strand β16. Motifs II, III and IV adopt new conformations. The color code defined in Figure 4A is also used here.

(Ser142). It seems that there is a correlation between these two backbone conformations and the side chain orientation of Glu267, a conserved residue crucial for the catalytic mechanism (Zhang *et al*, 2000; Lee *et al*, 2002; Zhang and Cheng, 2003). In PRMT1 and RMT1/Hmt1 that display an 'up' conformation, the last glutamic acid residue of motif III points away from the catalytic center, whereas in CARM1 and PRMT3 it points towards it.

Excluding the disorder to order transition of motif I, a few side chain rearrangements occur nevertheless upon SAH binding in the catalytic site of CARM1$_{140–480}$. They primarily affect the residues involved in the recognition of the methionine moiety, Arg169, Glu258, Gln160 and Met269. In absence of co-factor, the carboxylate group of Glu258 occupies the binding site of the carboxylate atoms of the SAH molecule. Fine structural changes and water molecule movements in the active site will be published elsewhere.

CARM$_{28–507}$ reveals a wobbly N-terminal domain

CARM1$_{28–507}$ was expressed using recombinant baculovirus, purified and crystallized as already published (Troffer-Charlier *et al*, 2007). The structure has been solved and refined at 2.55 Å (see Supplementary data for structure determination details and Table I for crystallographic statistics). Two regions of the polypeptide are not visible in the electron density map, namely residues 28–146 and 479–507. The absence of residues (28–146) in the electron density map of CARM1$_{28–507}$ crystals prompted us to carefully analyze the content of crystal to exclude proteolysis of the protein during the crystallization process. This has been performed by four different techniques: SDS polyacrylamide gel electrophoresis, N-terminal sequencing and MALDI mass spectrometry analysis on the purified protein and on dissolved crystals, and mass spectrometry under denaturing conditions on the purified protein (see Supplementary data). All techniques confirm the integrity of the protein at the end of the purification process and in the crystals and we will therefore keep the name CARM1$_{28–507}$ for this construct.

The missing electron density in CARM1$_{28–507}$ crystals (for residues 28–146 and residues 479–507) corresponds to two different origins of what is generally named disorder. At the C-terminal end, missing electron density for residues 479–507 probably means intrinsic disorder, which was indeed predicted by sequence analysis (Linding *et al*, 2003). The structure of CARM1$_{28–140}$ shows that residues 28–130 are ordered and fold as a PH domain. Therefore, missing electron density for those residues in the structure of CARM1$_{28–507}$ indicates that the PH domain assumes different positions, moves as a

rigid body and thus fails to scatter X-ray coherently. This means that the PH domain of CARM1 behaves as a wobbly domain (Dunker *et al*, 2001) connected by a flexible linker to the PRMT catalytic core (residues 140–480) and that both domains may behave independently. Nevertheless, they may cooperate upon binding to one or several other proteins as expected during coactivation of gene expression.

CARM1$_{28–507}$ reveals large structural changes in the catalytic site of PRMTs

In this work, we have solved the apo structure of the protein methyltransferase domain of CARM1 using two different constructs, CARM1$_{140–480}$ and CARM1$_{28–507}$. Those constructs reveal and illustrate two different types of structural changes occurring upon SAH binding and can therefore be analyzed in the light of the structure of SAH-CARM1$_{140–480}$. Two major structural changes are observed in CARM1$_{28–507}$ and concern the conformation of (i) peptide 147–179 and (ii) the four motifs characteristic of PRMTs.

In SAH-CARM1$_{140–480}$, the N-terminal peptide is structured into three helices αX (residues 144–154), αY (residues 157–164) and αZ (residues 167–178) as it has also been observed in PRMT3 (Zhang *et al*, 2000) (αX is not ordered in the structure of PRMT1 (Zhang and Cheng, 2003)). For those three helices, the angle between the axes of two consecutive helices is around 120° and plane (αX and αY) makes an angle of roughly 90° with plane (αY and αZ) (Figures 4A and 6B). In CARM1$_{28–507}$, residues 148–152 form a β-strand (named β0), followed by a turn of 3_{10} helix (residues 153–155) and residues 159–179 have been merged into a single long helix. To summarize, part of helix αX has been changed in a β-strand and the kink between helices αY and αZ has disappeared, helices αY and αZ have been merged together. Moreover, strand β0 forms a two-stranded antiparallel β-sheet with strand β16 located at the C-terminal end of the protein (Figure 5D). Superimposing residues 160–478 (the PRMT core domain, excluding motif I) of CARM1$_{28–507}$ with equivalent residues of SAH-CARM1$_{140–480}$ leads to an r.m.s. deviation between corresponding Cα atoms of 2.25 Å. Global conforma-

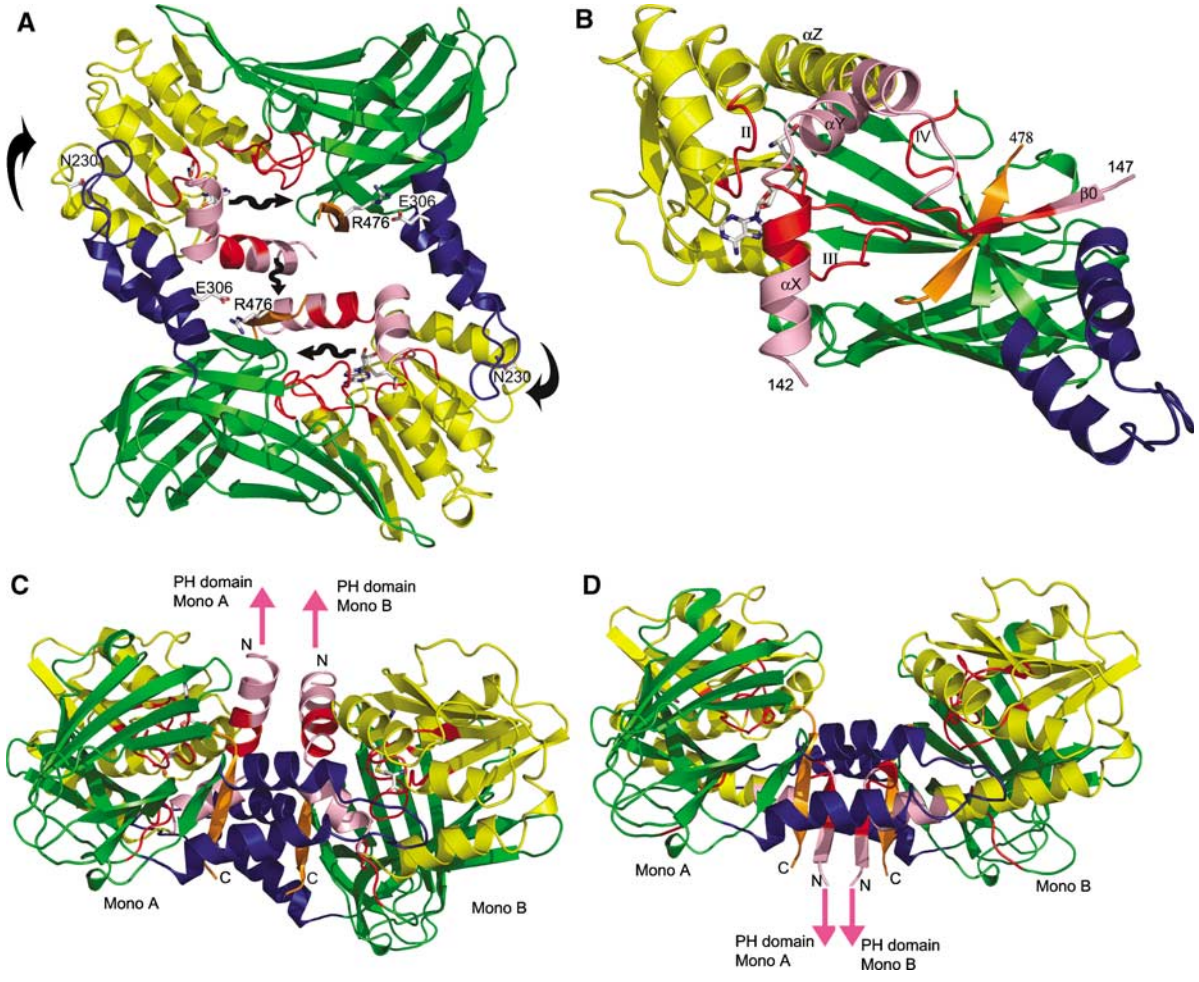

Figure 6 (**A**) Communication pathways in CARM1 dimer. The arrows schematize the hypothetical pathways inside a monomer and between monomers. (**B**) Structural changes at the N-terminal end of the PRMT catalytic domain of CARM1, which will lead to different position of the PH domain with respect to the PRMT catalytic domain. For clarity, schematic diagram of one monomer of SAH-CARM1$_{140–480}$ is shown and for CARM1$_{28–507}$ only β-strand β0 and helix (αY + αZ) of the corresponding monomer are shown. Strand β0 is antiparallel to β-strand β16 in CARM1$_{28–507}$. (**C**) Noncrystallographic SAH-CARM1$_{140–480}$ dimer indicating the putative global position of the wobbly PH domain. (**D**) Crystallographic CARM1$_{28–507}$ dimer indicating the putative global position of the PH domain. Monomer A of crystallographic CARM1$_{28–507}$ dimer and monomer A of noncrystallographic SAH-CARM1$_{140–480}$ dimer have been superimposed and shown in the same orientation.

tional change can be described as a small hinge movement of the two domains (Rossmann fold and β-barrel).

The structure of $CARM1_{28–507}$ also reveals a conformational change of the three other conserved motifs in the PRMTs core domain. As described above, in all other known crystal structures of PRMT catalytic domain, motifs III and IV have conserved backbone conformations that seem to be a prerequisite for catalytic activity. In $CARM1_{28–507}$, motif II and, surprisingly, motifs III and IV adopt new conformations that have not been seen before (Figure 5D). In summary, $CARM1_{28–507}$ reveals a structural rearrangement of all motifs of the core PRMT catalytic domain, which certainly corresponds to a nonproductive active site. It is surprising that this nonactive conformation has not been observed with apo-$CARM1_{140–480}$. It may mean that a molecular switch between active and inactive conformations exists and is correlated to the conformation of the N-terminal end of the protein and more specifically to the presence of the kink between helices αY and αZ. This kink contains Asp166, a highly conserved residue in all PRMTs sequences. Asp166, located just after motif I, interacts with His415, another highly conserved residue in all PRMTs sequences belonging to motif IV. It seems therefore that this kink is a pathway of communications between motifs I and IV. Any modification of the conformation of motif IV can be transmitted to motif III located nearby in the structure, and any modification of motif I at the level of the kink can be transmitted to motif II also nearby. In $CARM1_{28–507}$, helices αY and αZ are fused together and the kink does not exist anymore. The highly conserved interaction between Asp166 and His415 is replaced by a stacking interaction also involving two highly conserved residues in PRMTs sequence, Arg169 and Trp416. The conformational changes of motif I (namely residues 148–152) from an α-helix to a β-strand (β0), and the formation of a two-stranded antiparallel β-sheet between β0 and β16, position helices αY and αZ in line and force them to merge together.

It is surprising that those structural modifications have not been seen in apo $CARM1_{140–480}$, in which residues 142–154 are present (as confirmed by the structure of SAH- $CARM1_{140–480}$) but disordered. Crystallization conditions or crystal packing effects may of course sometimes produce biological artefacts. The crystals of $CARM1_{28–507}$ belong to the hexagonal space group $P6_222$ with one molecule in the asymmetric unit. Nevertheless, a crystallographic dimer can be generated that is similar to the noncrystallographic dimer observed in $CARM1_{140–480}$. A packing interaction exists between residue 158 (located just before the merged helix (αY-αZ)) of one monomer and residue 150 (located in strand β0) of one crystallographic equivalent molecule. However, this cannot be the driving force to produce the formation of the observed conformational change. $CARM1_{28–507}$ has been crystallized in the presence of 100 mM benzamidine chloride. Few molecules of benzamidine have been localized in the electron density map and one of them is located just nearby motif III inside the hydrophobic core of the β-barrel. This binding may be responsible for the modification of the conformation of motif III and the changes may have been transmitted to other motifs via the communication pathways described above and leading to a nonproductive active site. This observation opens new questions on methyl transferase inhibition and requires further investigations. Nevertheless, as discussed below, we would like to propose the hypothesis that this molecular switch (inactive conformations of the motifs, secondary structure rearrangement and β-sheet formation) may illustrate how CARM1 may regulate its biological activities by protein–protein interactions.

Communication pathways inside CARM1 PRMT catalytic dimer

Dimer formation has been shown to be a conserved feature in the PRMT family and indeed the PRMT core of CARM1 forms a similar dimer as observed in PRMT1, PRMT3 and yeast RMT/hmt1. It has been proposed that the dimer structure is necessary to build up the productive SAM-binding site and to allow processive production of the final methylation product, asymmetric dimethylarginine. CARM1 catalytic core can be noncrystallograhic dimer (as observed in $CARM1_{140–480}$) or crystallographic dimer ($CARM1_{28–507}$). As expected, the dimer formation involves interactions between the so-called dimerization arm of one monomer (residues 300–338 in CARM1) and the solvent exposed faces of the Rossmann fold helices (αY, αZ, αA and αB) of the other monomer (Figure 6).

As described above (Figure 3), sequence comparisons of the PRMT core of CARM1 (residues 150–471) with PRMT1 (36–354), PRMT3 (218–529) and RMT/hmt1 (21–349) show that CARM1 mainly contains an insertion peptide located between helices F and G of the dimerization arm. Despite a similar dimerization mode, dimers of core PRMTs CARM1, PRMT1, PRMT3 or RMT/hmt1 cannot be superimposed. Comparisons of CARM1 dimers with PRMT1, PRMT3 or RMT/hmt1 show that superimposition of one monomer leads to a rotation and a translation of the other monomer. This is also true for $CARM1_{28–507}$ and $CARM1_{140–480}$. Comparison of apo $CARM1_{140–480}$ dimer with SAH-$CARM1_{140–480}$ dimer shows that one monomer has rotated approximately by 2.5° with respect to the other monomer in the dimer. Comparison of apo SAH-$CARM1_{140–480}$ dimer with $CARM1_{28–507}$ crystallographic dimer, shows that one monomer has rotated approximately by 13° with respect to the other monomer in the dimer. Full details analysis of these changes in CARM1 dimers requires distinguishing properly between crystal packing effects and biological significative differences.

As the dimer structure seems important for protein methyltransferase activity, it should therefore exist signal communication pathways between the dimer interface and the catalytic center. The crystal structure of CARM1 reveals that three communication pathways may exist and transmit any modification of the active site to the dimer interface. As described above, the active site entrance of CARM1 is delineated on one side by helices αX and αY, on the top by helix αZ and by the loop of motif IV, and on the other side by strand β16.

The first pathway, as observed and described by other authors, uses the mainly hydrophobic dimer interface (Figure 6A) that involves three regions of one monomer (residues 155–178 (αX, αY), 195–206 (αA), 218–232 (αB)) and the dimerization arm of the other monomer. Several polar interactions also build up this interface, and many of them are idiosyncratic to each PRMT protein. One interaction involving Asn230, an invariant PRMT residue, and the main chain atoms of the other monomer is conserved in all known PRMT structures. The second pathway has not been de-

scribed before, as it implicates the last β-strand β16 of CARM1. Molecular events in the catalytic center may be transmitted on the other side of the active site through motifs III and IV and strand β16. Inside a given monomer, a salt-bridge interaction, involving Arg476 and Glu306, two residues conserved in CARM1 sequences, links strand β16 to the dimerization arm. A third pathway involves helix αX of each monomer. Helix αX of monomer 1 is approximately perpendicular to helix αX of monomer 2 and few interactions are seen between the first turn of each helix and brings extra stabilization to the dimer. Structural changes that occur inside one catalytic center can therefore be transmitted to the other catalytic site using those communication pathways.

Although dimerization (or oligomerization) is necessary to carry out methyltransferase activity, the dimer may not always be the biological active structure of CARM1 as recently proposed for PRMT1 (Lee *et al*, 2007). Surface-scanning analysis of PRMT1 suggested that full or at least partial dissociation of the dimer (or oligomer) is necessary to bind GRIP1. Similar phenomena may exist for CARM1 and the pathways between monomers described above may be important as they highlight ways to modify the productive catalytic dimer and therefore probably regulate the methyltransferase activity.

Functional implications and conclusion

CARM1 architecture has been schematically divided into three structural domains, a catalytic core domain to which two unique additional domains are appended, respectively, at the N- and C-terminal sides of the PRMT active site. Bioinformatics analysis of CARM1 sequences, cloning, expression and purification assays of many constructs containing one or several regions of mCARM1 lead us to eventually solve the structure of three isolated modules of mCARM1: $CARM1_{28–140}$, $CARM1_{140–480}$ and $CARM1_{28–507}$. From sequences analysis, the first 25 amino acids and the last 120 amino acids are predicted to be highly disordered. Despite extensive efforts, it has not been possible to overexpress, obtain in a soluble state and purify in quantities or concentrations compatible with structural studies any constructs encompassing those disordered regions. Moreover, at least in our hands, constructs containing the C-terminal domain of mCARM1 are prone to proteolysis (data not shown). All those data prompted us to hypothesize that the C-terminal domain of mCARM1 is mainly unfolded in a free state and that a disorder to order transition will take place upon binding to one or several partners. CARM1 is therefore another example of natively disordered protein and can be divided into five parts: two intrinsically disordered regions (residues 1–25, residues 480–607), a wobbly PH domain (residues 28–130), a small linker (residues 131–140) and PRMT catalytic domain (residues 141–480).

In this work, we have solved the structure of the N-terminal domain of CARM1. $CARM1_{28–140}$ adopts a PH domain-like fold, a very common structural scaffold that has been found in a broad range of proteins with diverse enzymatic and regulatory activities (Kwek *et al*, 2004). Among PH domains, $CARM1_{28–140}$ is highly similar to EVH1 domains. As discussed above, although the PH domain of CARM1 shares structural similarity with EVH1 and other PH domains, there is no sequence similarity with any known class. Moreover, the ligand-binding site found in other PH domains is involved in the formation of $CARM1_{28–140}$ dimer. Therefore, if $CARM1_{28–140}$ dimer is not biologically relevant, the ligand recognized by CARM1 PH domain may differ from those already known and remains to be discovered.

We have also solved the structure of the PRMT catalytic domain of mCARM1 in three different contexts: an apo $CARM1_{140–480}$, a SAH-$CARM1_{140–480}$ and an apo $CARM1_{28–507}$. Those constructs reveal and illustrate two different types of structural changes occurring upon SAH binding and can therefore be analyzed in the light of the structure of SAH-$CARM1_{140–480}$. Comparison of apo $CARM1_{140–480}$ with SAH-$CARM1_{140–480}$ shows an order to disorder transition of the N-terminal helix αX of CARM1. In all crystal structures, a dimer (crystallographic or non-crystallographic) of CARM1, which is similar to other known PRMT structures, is observed. The structures of CARM1 reveal that a β-strand (β16) located at the C-terminal end of the PRMT core, and not observed in other PRMT structures, has to be considered as an essential feature of the CARM1 active site. Comparison of the two apo conformations, $CARM1_{140–480}$ and $CARM1_{28–507}$, reveals a conformational change of the four motifs characteristic of PRMTs and a secondary structure change of helices αX, αY and αZ. Part of helix αX has been changed in a β-strand (β0) that interacts with the C-terminal strand β16. The observation may illustrate two aspects with biological relevance. It first shows how protein–protein interactions may lead to a nonproductive active site. As β16 is an integral part of the active site, we can also hypothesize that the two-stranded antiparallel β-sheet (β0–β16) observed in $CARM1_{28–507}$ mimics the interaction between CARM1 and a potential substrate. As CARM1 has been shown to methylate different substrates, with apparently no consensus motif, backbone interactions can increase affinity without itself imposing specificity, and therefore may modulate affinity of different partners for the same binding site (Remaut and Waksman, 2006). Finally, communication pathways that transmit any modification of the active site to the dimer interface may be found.

The $CARM1_{28–507}$ structure reveals that residues 28–146, which have been proven to be present in the crystallized protein, are not seen in the electron density map. Therefore, the N-terminal PH domain of CARM1 behaves as a wobbly domain connected by a flexible linker to the PRMT catalytic core (residues 140–480). Nevertheless, they may cooperate upon binding to one or several other proteins as expected during coactivation of gene expression.

The crystal structures of catalytic domain of PRMTs did not show how full-length proteins will dimerize (or oligomerize). Analyses of our crystal structures of CARM1 PRMT domain show how dimers of CARM1 catalytic core can be assembled to form octamer as sometimes observed in solution (data not shown). The crystal of $CARM1_{28–140}$ dimer reveals how the N-terminal domain of CARM1 may dimerize. However, the structural changes at the N-terminal end of CARM1 PRMT catalytic domain observed in SAH-$CARM1_{140–480}$ and $CARM1_{28–507}$ lead to different putative positions of the PH domain (Figure 6B). In orientation of Figure 6C, the PH domain of each SAH-$CARM1_{140–480}$ monomer would be located on the top part of the figure. Using a similar orientation for the $CARM1_{28–507}$ dimer, the PH would be located on the bottom part of the figure (Figure 6D). Those alternative locations of the PH domain are not interchangeable after

the formation of the PRMT catalytic dimer, as movement from one location to the other requires the dissociation of the dimer. The biological signification of those alternative positions remains to be proven. As already mentioned, the stabilization of the wobbly PH domain in its functional position will probably require the presence of other partners. Further insights will come from the structures of binary or ternary complexes, including full-length CARM1 and protein substrates.

CARM1 is a key player in the formation of large complexes on gene promoters and the work presented in this paper is only a first step of a process aimed at understanding at the atomic level the cooperative mechanism by which CARM1 plays its biological functions. Our work provides atomic structure of CARM1 modules that constitute a starting point for future interactions studies and a foundation for further functional studies. X-ray crystallography is challenged to produce a yearned image of several multiprotein complexes involving CARM1 to understand how protein methylation is controlled or regulated in the formation (or dissociation) of large and dynamic complexes.

Materials and methods

Protein expression and crystallization

Details of the expression, purification and crystallization of $CARM1_{28–140}$ are given in the Supplementary data. $CARM1_{28–507}$, apo and SAH-$CARM1_{140–480}$ have been overexpressed, purified and crystallized as already published (Troffer-Charlier *et al*, 2007).

Data collection, structure determination and refinement

The structure of $CARM1_{28–140}$ has been solved as described in the Supplementary data. The current refined model has a crystallographic R-factor of 20.5% (Rfree = 25.5%) at 1.7 Å resolution (see Table I for detailed statistics). Data collection and initial structure determination of $CARM1_{28–507}$ and $CARM1_{140–480}$ have been already published (Troffer-Charlier *et al*, 2007). The structure of $CARM1_{28–507}$ has been solved as described in the Supplementary data. The structures of Apo $CARM1_{140–480}$ and SAH-$CARM1_{140–480}$ were solved by molecular replacement methods using the corresponding isolated domain extracted from the previously solved $CARM1_{28–507}$ structure as a probe with MOLREP (CCP4, 1994). Apo $CARM1_{140–480}$ crystals belong to the orthorhombic space group I222 and contain two molecules in the asymmetric unit. The final model contains two copies, designated as molecules A and B, respectively. Two regions of the polypeptide are not visible in the electron density map and are assumed to be disordered, namely residues 140–154 and 479–480 for molecule A and B. The current refined model has a crystallographic R-factor of 20.5% (Rfree = 26.5%) at 2.4 Å resolution (see Table I for detailed statistics).

SAH-$CARM1_{140–480}$ crystals, obtained by co-crystallization in the presence of the cofactor product SAH, belong to the orthorhombic space group $P2_12_12$ and contain four molecules in the asymmetric unit. Residues 140–141, the first two residues at the N-terminal side of $CARM1_{140–480}$ and residues 479–480, the last two residues at the C-terminal side of $CARM1_{140–480}$, are not visible in the electron density map and are assumed to be disordered. The current refined model has a crystallographic R-factor of 18.6% (Rfree = 23.9%) at 2.2 Å resolution (see Table I for detailed statistics).

Despite the fact that the crystals of the apo and holo forms of $CARM1_{140–480}$ have been obtained in very similar mother liquor condition, they correspond to two different space groups with nevertheless very close unit cell dimensions. Crystals of apo-$CARM1_{140–480}$ contain one dimer in the asymmetric unit, whereas crystals of SAH-$CARM1_{140–480}$ contain two dimers in the asymmetric unit. In the $P2_12_12$ holo form, the two dimers are related by a noncrystallographic fractional translation of ($\sim$0.47, 0.50, 0.50) resulting in a pseudo-I222 packing. This space group transition is due to a slight modification of the dimer, resulting from a rotation of roughly 2.3° of one monomer relative to the other.

Refinements were performed with REFMAC5 (CCP4, 1994) and iterative models building with O (Kleywegt and Jones, 1996) and Coot (Emsley and Cowtan, 2004). All other crystallographic calculations were carried out with the CCP4 package (CCP4, 1994). The stereochemistry of all models was inspected by Procheck (Laskowski *et al*, 1993) and the quality of the refined structures was assessed using the Biotech validation suite for Protein structures (Vriend, 1990; Wodak *et al*, 1995). The refinement statistics are summarized in Table I. Molecular graphics figures were generated using PyMOL (DeLano, 2002).

Supplementary data

Supplementary data are available at *The EMBO Journal* Online (http://www.embojournal.org).

Acknowledgements

We thank members of the ESRF-EMBL Joint Structural Biology Group for use of the ESRF beamline facilities and help during data collection. We thank H Nierengarten for Mass spectrometry and M Argentini for Maldi peptide mass finger printing. The work described here was supported by funds from Association pour la Recherche sur le Cancer (contracts N°3230 and N°3910), and the European Commission as SPINE2-complexes contract n° LSHG-CT-2006–031220.

References

Ball LJ (2005) EVH1/WH1 domains. In *Modular Protein Domains*, Cesareni G, Gimona M, Sudol M, Yaffe M (eds), pp 73–100. Weinheim: Wiley-VCH Verlag GmBH & Co. KGaA

Ball LJ, Jarchau T, Oschkinat H, Walter U (2002) EVH1 domains: structure, function and interactions. *FEBS Lett* **513:** 45–52

Bedford MT, Richard S (2005) Arginine methylation an emerging regulator of protein function. *Mol Cell* **18:** 263–272

Beitz E (2000) TEXshade: shading and labeling of multiple sequence alignments using LATEX2 epsilon. *Bioinformatics* **16:** 135–139

Blomberg N, Baraldi E, Nilges M, Saraste M (1999) The PH superfold: a structural scaffold for multiple functions. *Trends Biochem Sci* **24:** 441–445

CCP4 (1994) The CCP4 suite: programs for protein crystallography. *Acta Crystallogr D* **50:** 760–763

Chen D, Ma H, Hong H, Koh SS, Huang SM, Schurter BT, Aswad DW, Stallcup MR (1999) Regulation of transcription by a protein methyltransferase. *Science* **284:** 2174–2177

Cheng D, Cote J, Shaaban S, Bedford MT (2007) The arginine methyltransferase CARM1 regulates the coupling of transcription and mrna processing. *Mol Cell* **25:** 71–83

Cheng X, Collins RE, Zhang X (2005) Structural and sequence motifs of protein (histone) methylation enzymes. *Annu Rev Biophys Biomol Struct* **34:** 267–294

DeLano WL (2002) *The PyMOL User's Manual*. San Carlos, CA, USA: DeLano Scientific

Dunker AK, Lawson JD, Brown CJ, Williams RM, Romero P, Oh JS, Oldfield CJ, Campen AM, Ratliff CM, Hipps KW, Ausio J, Nissen MS, Reeves R, Kang C, Kissinger CR, Bailey RW, Griswold MD, Chiu W, Garner EC, Obradovic Z (2001) Intrinsically disordered protein. *J Mol Graph Model* **19:** 26–59

Emsley P, Cowtan K (2004) Coot: model-building tools for molecular graphics. *Acta Crystallogr D* **60:** 2126–2132

Engh RA, Huber R (1991) Accurate bond and angle parameters for X-ray protein structure refinement. *Acta Crystallogr A* **47:** 392–400

Feng Q, Yi P, Wong J, O'Malley BW (2006) Signaling within a coactivator complex: methylation of SRC-3/AIB1 is a molecular switch for complex disassembly. *Mol Cell Biol* **26:** 7846–7857

Gervais V, Lamour V, Jawhari A, Frindel F, Wasielewski E, Dubaele S, Egly JM, Thierry JC, Kieffer B, Poterszman A (2004) TFIIH contains a PH domain involved in DNA nucleotide excision repair. *Nat Struct Mol Biol* **11:** 616–622

Holm L, Sander C (1995) Dali: a network tool for protein structure comparison. *Trends Biochem Sci* **20:** 478–480

Kleywegt GJ, Jones TA (1996) Efficient rebuilding of protein structures. *Acta Crystallogr D* **52:** 829–832

Krause CD, Yang ZH, Kim YS, Lee JH, Cook JR, Pestka S (2007) Protein arginine methyltransferases: Evolution and assessment of their pharmacological and therapeutic potential. *Pharmacol Ther* **113:** 50–87

Kwek KY, O'Gorman W, Akoulitchev A (2004) Transcription meets DNA repair at a PH domain. *Nat Struct Mol Biol* **11:** 588–589

Laskowski RA, Mac Arthur MW, Moss DS, Thornton JM (1993) PROCHECK: a program to check the stereochemical quality of protein structures. *J Appl Crystallogr* **26:** 283–291

Lee DY, Ianculescu I, Purcell D, Zhang X, Cheng X, Stallcup MR (2007) Surface-scanning mutational analysis of protein arginine methyltransferase 1: roles of specific amino acids in methyltransferase substrate specificity, oligomerization, and coactivator function. *Mol Endocrinol* **21:** 1381–1393

Lee YH, Koh SS, Zhang X, Cheng X, Stallcup MR (2002) Synergy among nuclear receptor coactivators: selective requirement for protein methyltransferase and acetyltransferase activities. *Mol Cell Biol* **22:** 3621–3632

Lemmon MA (2007) Pleckstrin homology (PH) domains and phosphoinositides. *Biochem Soc Symp* **74:** 81–93

Lemmon MA, Ferguson KM, Abrams CS (2002) Pleckstrin homology domains and the cytoskeleton. *FEBS Lett* **513:** 71–76

Linding R, Russell RB, Neduva V, Gibson TJ (2003) GlobPlot: exploring protein sequences for globularity and disorder. *Nucleic Acids Res* **31:** 3701–3708

Martin JL, McMillan FM (2002) SAM (dependent) I AM: the *S*-adenosylmethionine-dependent methyltransferase fold. *Curr Opin Struct Biol* **12:** 783–793

Murzin AG, Brenner SE, Hubbard T, Chothia C (1995) SCOP: a structural classification of proteins database for the investigation of sequences and structures. *J Mol Biol* **247:** 536–540

Naeem H, Cheng D, Zhao Q, Underhill C, Tini M, Bedford MT, Torchia J (2007) The activity and stability of the transcriptional coactivator p/CIP/SRC-3 are regulated by CARM1-dependent methylation. *Mol Cell Biol* **27:** 120–134

Pahlich S, Zakaryan RP, Gehring H (2006) Protein arginine methylation: cellular functions and methods of analysis. *Biochim Biophys Acta* **1764:** 1890–1903

Remaut H, Waksman G (2006) Protein–protein interaction through beta-strand addition. *Trends Biochem Sci* **31:** 436–444

She M, Decker CJ, Sundramurthy K, Liu Y, Chen N, Parker R, Song H (2004) Crystal structure of Dcp1p and its functional implications in mRNA decapping. *Nat Struct Mol Biol* **11:** 249–256

Teyssier C, Chen D, Stallcup MR (2002) Requirement for multiple domains of the protein arginine methyltransferase CARM1 in its transcriptional coactivator function. *J Biol Chem* **277:** 46066–46072

Troffer-Charlier N, Cura V, Hassenboehler P, Moras D, Cavarelli J (2007) Expression, purification, crystallization and preliminary crystallographic study of isolated modules of the mouse coactivator-associated arginine methyltransferase 1. *Acta Crystallograph Sect F Struct Biol Cryst Commun* **63:** 330–333

Vriend G (1990) WHATIF: a molecular modelling and drug design program. *J Mol Graph* **8:** 52–56

Weiss VH, McBride AE, Soriano MA, Filman DJ, Silver PA, Hogle JM (2000) The structure and oligomerization of the yeast arginine methyltransferase, Hmt1. *Nat Struct Biol* **7:** 1165–1171

Wodak SJ, Pontius J, Vaguine A, Richelle J (1995) Validating protein structures. From consistency checking to quality assessment. In *Proceedings of the CCP4 Daresbury Study Weekend: 'Making the most of your model'*, pp 41–51. Warrington, UK: SERC Daresbury Laboratory

Wysocka J, Allis CD, Coonrod S (2006) Histone arginine methylation and its dynamic regulation. *Front Biosci* **11:** 344–355

Xu W, Cho H, Kadam S, Banayo EM, Anderson S, Yates III JR, Emerson BM, Evans RM (2004) A methylation-mediator complex in hormone signaling. *Genes Dev* **18:** 144–156

Zhang X, Cheng X (2003) Structure of the predominant protein arginine methyltransferase PRMT1 and analysis of its binding to substrate peptides. *Structure (Camb)* **11:** 509–520

Zhang X, Zhou L, Cheng X (2000) Crystal structure of the conserved core of protein arginine methyltransferase PRMT3. *EMBO J* **19:** 3509–3519